Pore Structure and Particle Size Effects on Limestone Capacity for SO_2 Removal

A detailed investigation of the dependence of the transient behavior of limestone particles reacting with SO_2 in the presence of oxygen on the pore structure properties of the calcined solid is presented. Experimental reactivity and pore structure data were obtained for two high-purity limestones that yield calcines of qualitatively similar distribution of pore size but of different capacity for SO_2 removal. Experiments were carried out over a wide range of particle size and temperature so as to investigate the effects of intraparticle mass transport limitations on the process. The results obtained showed strong dependence of the transient behavior of reacting particles of calcined limestone, and consequently of their sorptive capacity for SO_2 removal, on their initial pore size distribution and on the resistance for intraparticle mass transport—which is also determined to a certain extent by the pore size distribution. The experimental results were found to be in agreement with the predictions of a mathematical model for gas-solid reactions with solid product involving porous solids of distributed pore size. The findings point to the conclusion that the evaluation of limestones proposed for use as sorbents for controlling SO_2 emissions should be based on the size distribution and interconnectedness of the pores of their calcines and not only on their average structural properties (porosity and surface area).

Solon Zarkanitis
Stratis V. Sotirchos
Department of Chemical Engineering
University of Rochester
Rochester, NY 14627

Introduction

Limestone and dolomite find extensive use in the control of emissions of sulfur dioxide (SO_2) from coal-fired power plants. In the high-temperature environment of a combustor, the limestone or dolomite particles undergo calcination, and the calcined product (CaO or MgO) reacts with the sulfur dioxide produced during coal combustion, forming calcium or magnesium sulfate. (Sulfides and sulfites may also be formed at reaction temperatures lower than 750°C: Chan et al., 1970; Marsh and Ulrichson, 1985). One of the most interesting aspects of the reaction of calcined limestone or dolomite with SO_2 as a gas-solid reaction is the formation of a solid product (calcium sulfate or magnesium sulfate) which stoichiometrically occupies considerably more volume (three to four times more) than the solid reactant (calcium oxide or magnesium oxide) from which it results. The formation of the solid product leads to complete pore plugging in the interior of the reacting particles, and consequently the sulfation reaction may be effectively stopped before complete utilization of the sorbent takes place. Pores of different size are expected to be plugged at different times, with the smallest pores being filled with solid product first. The transient behavior of the reacting limestone particles should therefore depend in general not only on the average structural properties of the porous calcined solid (internal surface area and porosity) but on the form of the pore size distribution as well, even under reaction conditions characterized by negligible intraparticle concentration gradients.

In the presence of significant intraparticle diffusional limitations, the overall picture of the reaction of calcined limestone or dolomite with SO_2 becomes considerably more complex. Because of higher rate of reaction at the external surface of the particles, complete pore closure may first take place at the external surface while there is still open pore space left in the interior. For obvious reasons, such an event can lead to ultimate SO_2 capacities that are much lower than those predicted by the stoichiometry of the reaction for complete plugging of the internal pore space. A possible remedy to this situation would be the use

Correspondence concerning this paper should be addressed to S. V. Sotirchos.

of sorbents with pore size distributions shifted toward large pore sizes, but such a solution involves considerable loss of internal surface area, and as a result it may lead to unacceptably low reactivities. Another alternative would be to use sorbents with broader distribution of pore size, but such a choice presents the disadvantage of bringing most of the available for reaction internal surface area in the range of small pores. As a result, the reactivity of the solid may start experiencing a drastic decrease at the conversion level where closure of the small pores begins to take place. Because of the above complications, it can be said that it is practically impossible to identify optimal pore structures of calcined solids for SO_2 removal without considering the operating conditions under which the sulfation reaction is expected to be carried out.

Most of the above intuitive observations have been more or less verified by various distributed-pore models for gas-solid reactions with solid product recently presented in the literature (Christman and Edgar, 1983; Sotirchos and Yu, 1985; Yu and Sotirchos, 1987). For instance, it was found (Sotirchos and Yu, 1985) that sorbents with bimodal pore size distribution may exhibit considerably lower sorptive capacities than sorbents with narrower distribution of pore size, even if the former are initially characterized by higher internal surface areas and intraparticle diffusional limitations are absent. However, although the calcination and sulfation reactions of limestone and dolomite have been the subject of extensive experimental investigation, unambiguous experimental evidence that leads to a clear understanding of the effects of pore size distribution of calcined stones on their capacity for SO_2 removal is still lacking. Most of the initial studies concentrated on determining the global kinetics of the sulfation reaction and the sulfation capacities of various stones (Harrington et al., 1968; Borgwardt, 1970) while paying little attention to the pore structure of the calcined solid. It was soon realized that the intrinsic kinetics of the reaction were masked both by the intraparticle diffusional limitations and the diffusion process in the solid product, and reports began of values for the internal surface area and the porosity of the calcined solid.

A broad spectrum of limestones and dolomites consisting of eleven specimens was studied by Borgwardt and Harvey (1972). Their results showed that the reactivity of small particles (about 96 μm) for a certain stone increased in proportion to the internal surface area, which was varied by changing the calcination temperature. However, the data showed little correlation among the reaction rates and SO_2 capacities of different stones and the reported surface area and initial porosity values. The effects of the calcination temperature on the pore size distribution, and hence on the sorptive capacity of a limestone, were investigated by Dogu (1981), who also reported pore size distribution data. Particles of very large size (about 1 cm) were employed in Dogu's experiments, and therefore the effects of the pore size distribution on the local reactivity of the solid, if any, were overshadowed by those of the intraparticle diffusional limitations. It should be pointed out that although calcination at different temperatures can bring about considerable quantitative changes in the structural properties of the solid, its effects on the qualitative characteristics of the pore size distribution may be of rather limited extent.

In their experimental study of limestone sulfation, Hartman and Coughlin (1974, 1976) observed that limestones with a larger fraction of small pores could exhibit lower capacities for SO_2 removal. A large volume of data compiled by Hartman et al. (1978) on the saturation capacities of calcined limestones for SO_2 absorption showed that although the maximum capacity predicted by the stoichiometry of the reaction for complete pore closure offered a satisfactory upper bound on the capacity of calcined stones, the actual capacity had no clear relationship to the total pore volume. This suggested significant effects of the pore size distribution (not reported for most stones) or of the particle size used in the experiments (565 μm). Similar conclusions were also reached in the more extensive investigations of Vogel et al. (1977) and Hasler et al. (1984) (11 and 37 samples, respectively).

An experimental investigation of the dependence of the sulfation capacity of calcined limestones on factors related to pore size distribution and particle size is presented in our study. Experimental reactivity and pore structure data are reported for two high-purity limestones, which upon calcination yield products of similar distribution of pore size but of different capacity for SO_2 removal. As mentioned above, the pore size distribution of the solid may influence the overall reaction rate of gas-solid reactions with solid product not only through its effects on the local reactivity of the particles but through its effects on the intraparticle diffusional limitations as well. In order to be able to distinguish these two types of effects, reactivity experiments have been carried out over rather wide ranges of particle size (50–350 μm) and calcination and sulfation temperature (700–850°C).

Experimental Details

Reactivity measurements for both calcination and sulfation experiments were conducted in a thermogravimetric analysis (TGA) system. The main part of this system is a Cahn 2000 electrobalance housed in a three-port bell jar with one port connected to the reactor tube. It can handle weights up to 3.5 g and is sensitive to weight changes as small as 0.1 μg. The hangdown tube consists of two concentric quartz tubes, the inner of 19 mm ID, the other of 35 mm ID. The solid sample is placed in a 5 mm platinum pan suspended from the sample arm of the balance with thin platinum wire. The reactant gases enter the annular region through a 6 mm OD quartz tube, and then pass through the inner reactor tube, in which they react with the solid reactant. The effluent gases are then purged through a side port of the outer reactor tube. In order to protect the weighing unit from contamination, inert gas (N_2) is sent through the bell jar from a side port. A detailed description of the TGA system is given by Zarkanitis (1989).

The TGA apparatus is coupled with a vacuum system, and consequently it can also be used for physical adsorption measurements. The experimental arrangement basically remains the same when the apparatus is used for adsorption measurements, the only difference being that the side port of the bell jar is in this case used to connect it with the vacuum system. However, the pan configuration of the thermogravimetric analysis system makes it practically impossible to control the interparticle diffusional resistances in the relatively large samples needed for adsorption measurements; as a result, calcination may not take place uniformly throughout the sample. For this reason, physical adsorption measurements, for surface area determination, were carried out in a flow-type reaction/adsorption apparatus (Crowley, 1985; Sotirchos et al., 1988). This apparatus has been designed in such a way that calcination and gas adsorp-

tion experiments can be conducted on the same sample *in situ*. Since the calcined samples do not have to be transferred to a different apparatus for surface area determination, considerable reduction of the overall experimentation time is achieved. The device has been successfully used in the study of char gasification and combustion (Crowley, 1985; Sotirchos et al., 1988). The operation of the apparatus is based on a continuous flow method for physical adsorption measurements first proposed by Nelsen and Eggersten (1958). It is a well-established method for adsorption experiments that uses a thermal conductivity detector (TCD) to measure the gas concentration. The gas stream (He-N_2 mixture for surface area measurement, N_2 for calcination experiments) passes successively through the reference cell of the thermal conductivity detector, the reactor tube where adsorption or calcination takes place, and, finally, the sample cell of the TCD. A more detailed description of the apparatus is given elsewhere (Sotirchos et al., 1988).

Reactivity measurements for calcination and sulfation experiments were carried out using the TGA system. About 3 to 5 mg of limestone sample were placed in the platinum sample pan, and the sample was outgassed in CO_2 at 150°C. After outgassing, the sample was heated to the desired temperature. During the heating process, CO_2 was passed through the reactor tube to prevent decomposition of limestone, Inert gas (N_2) was sent at all times through the side port of the housing chamber to protect the weighing unit from contamination. When the temperature reached the desired value, a four-port switching valve was used to switch gaseous streams, sending pure N_2 through the hang-down tube where the sample was suspended. The weight of the solid was monitored continuously until stable weight was reached.

After the calcination reaction was completed, the calcined sample was used for the sulfation experiment. The sample was brought to the sulfation temperature, and a mixture of SO_2-air-N_2 was sent through the reactor tube, starting the sulfation reaction. Weight change data were collected for about 60 min. For all runs, both calcination and sulfation, the volumetric flow rate used for the gaseous mixture was 250 mL/min, which corresponded to a linear velocity of 90 cm/min in the inner tube.

In order to get enough sample for surface area and pore size distribution measurements, a quantity of 300–500 mg of limestone was used for the calcination experiments. For internal surface areas of 10 m^2/g or more, it was found that 250 mg of CaO (calcined from about 460 mg of limestone) was adequate for accurate and reproducible surface area measurement using our reaction/adsorption apparatus. Before the calcination started, the solid sample was outgassed in CO_2 at 150°C for about 30 min, and it was then heated to the reaction temperature under CO_2 so as to prevent decomposition of the limestone during the heating process. After the desired temperature was reached, N_2 was introduced through the reaction/adsorption system. The flow rate of the sweeping gas (N_2) was 100 mL/min and corresponded to a linear velocity of 830 cm/min in the reactor tube. The extent of the calcination reaction was continuously monitored using the output signal of the thermal conductivity detector. The extent of the calcination was double-checked by measuring the weight of the sample before and after the reaction.

The calcined sample was then used for gas adsorption measurements. Mixtures of helium and nitrogen were passed through the U-shaped reactor tube. When a stable baseline was reached by the signal of the thermal conductivity detector, the reactor tube was immersed in liquid nitrogen, and adsorption took place. The area under the peak of the signal of the TCD during adsorption or desorption (i.e., during withdrawal of the U-tube from the liquid nitrogen bath) was used to find the amount of nitrogen adsorbed or desorbed (Sotirchos et al., 1988).

Materials

Two limestone specimens were used in our experiments: a limestone of very high $CaCO_3$ content distributed by Greer Limestone Co. and a calcitic marble (Tate White Aggregate) distributed by Georgia Marble Co. The stones were crushed and then sieved to a variety of mesh sizes using a Fisher electric sieve shaker. Experiments were carried out for four ranges of particle size:

250–270 mesh (53–62 μm)
150–170 mesh (88–105 μm)
60–65 mesh (210–250 μm)
42–48 mesh (297–350 μm)

The reaction gases used in the calcination experiments were N_2 (99.995%) and CO_2 (99.99%). For the physical adsorption experiments, high-purity He (99.995%) was used as the carrier gas. The reaction gas used in the sulfation experiments was 5,000 ppm SO_2 in air, which was further diluted to 3,000 ppm SO_2 by mixing it with N_2. The gases were supplied by Air Products Co.

The stones were nearly nonporous in their natural state, as mercury porosimetry and photomicrographs obtained through scanning electron microscopy (SEM) showed. Mineralogical analysis of the two stones showed that the calcium carbonate was present in the form of calcite. Thin sections of the two stones were examined under a petrographic microscope. The Georgia marble sample was found to be primarily spanned by coarse calcitic grains. The Greer limestone sample, on the other hand, mainly consisted of calcitic, microgranular mud with inclusions of aggregates of small calcitic grains. At the boundaries of the grains, small grains of iron oxide and quartz were observed to occur in both stones. Highly porous samples were obtained after calcination. The average apparent density and porosity of Greer limestone (GL) particles after calcination were 1.58 g/cm^3 and 0.52, while the corresponding values for the calcined Georgia marble (GM) were 1.63 g/cm^3 and 0.51. The composition of the calcined products of the two stones is shown in Table 1. The

Table 1. Composition of Calcined Products

Oxide	Georgia Marble wt. %	Greer Limestone wt. %
CaO	94.16	97.34
MgO	2.57	0.81
SiO_2	2.62	1.5
Al_2O_3	0.14	0.18
Na_2O	0.01	0.01
K_2O	0.03	0.04
Fe_2O_3	0.06	0.08
MnO	0.01	0.01
TiO_2	0.03	0.04
P_2O_5	0.22	0.29
Total	99.85	100.30

analyses were performed by X-ray Assay Laboratories Ltd. Notice that the CaO content of the calcitic marble is slightly lower than that of the Greer limestone (94.16 vs. 97.34%), but the former contains more MgO—which might also react with SO_2.

Results and Discussion

Initial pore structure properties of the calcined samples

The calcined samples were found to exhibit type II or IV adsorption isotherms, according to BDDT classification (Gregg and Sing, 1982), and the BET method was employed for surface area estimation. Measured surface areas for various and calcination temperatures are given in Table 2. The surface area per unit mass of calcined sample decreased with increasing calcination temperature, as the results of Table 2 show, while there was practically no particle size effect. It is interesting to note that the surface area of the GM sample is smaller than that of the GL samples.

To assess the effects of sintering on the surface area of the calcined product, calcined dolomite and limestone samples obtained from calcination at 750°C were heat-treated in nitrogen at higher temperatures for about 30 min, and their surface area was again determined by the BET method. Surface areas were thus measured at two different temperatures, 750 and 850°C, for 88–105 μm particles (Table 2). This treatment had practically no effect on the surface area of the GL sample, as the results in Table 2 indicate, but it decreased the surface area of the GM sample from 40.0 m^2/g (750°C) to 38.4 m^2/g (850°C), probably because of structural changes associated with sintering. Although this change was relatively small, sulfation experiments were conducted at temperatures lower than the calcination temperature used to produce the calcines since otherwise, the initial pore structure properties of the calcined products might have little relation to their actual reactivity during the sulfation experiments. Such behavior is suggested by experiments conducted by Dogu (1981), who found that when samples calcined at 750°C were heated to 840°C for the sulfation reaction, their reaction behavior was similar to that of samples calcined at 850°C. Borgwardt et al. (1986) exploited the effect of sintering on the pore structure of the calcined solid to control the grain size of the solid phase.

The pore size distributions of the calcined samples were measured by mercury porosimetry using a Micromeritics porosimeter. The pore size distributions of Greer limestone samples calcined at two different temperatures (750 and 850°C) are shown in Figure 1 (curves *A*). The total porosity of the calcined product was about 0.52 and remained almost unchanged over this temperature range, as the results in Figure 1 show. However, the pore size distribution shifted to larger pore sizes as the calcination temperature increased from 750 to 850°C, and the most probable pore radius of the distribution increased from about

Table 2. Surface Areas of Calcined Samples

Calcination Temp. °C	Greer Limestone m^2/g	Georgia Marble m^2/g
750	47.8	40.0
850	33.7	32.3
750*	47.4	38.4

*Followed by treatment under N_2 for 30 min at 850°C

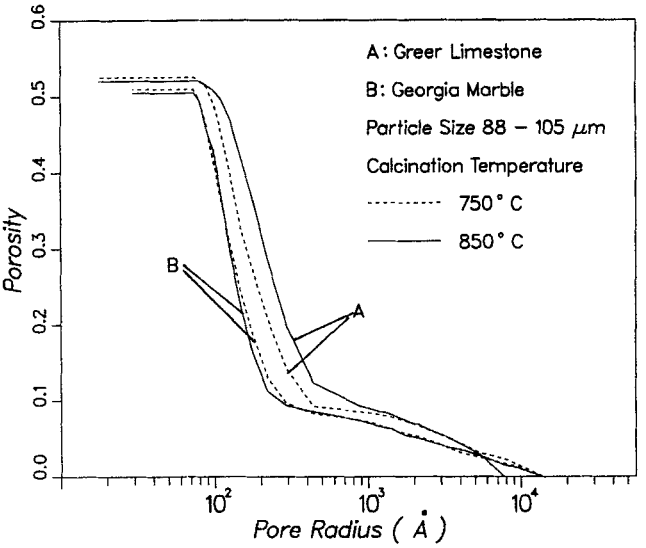

Figure 1. Pore size distributions of Greer limestone and Georgia marble samples.

140 to 210 Å. The behavior of the pore size distribution of the calcines of the Greer limestone sample was in qualitative agreement with the observed reduction of the internal surface area, by about 30%, as the calcination temperature was increased from 750 to 850°C.

The corresponding pore size distributions of calcined marble samples are also shown in Figure 1 (curves *B*). It was again found that the temperature had little effect on the total porosity of the calcined sample, which was found to have an average value of 0.51. The pore size distribution, on the other hand, showed no noticeable change as the calcination temperature was increased despite the fact that the total surface area predicted by the BET method decreased by about 20%, Table 2. As seen by comparing curves *A* and *B* of Figure 1, the pore size distributions of the Georgia marble calcines are characterized by much smaller pore sizes than those of the Greer limestone samples, with the most probable pore size located around 110 Å, although the BET internal surface areas of the latter are higher, Table 2. The above observations do not necessarily suggest a discrepancy between the mercury porosimetry and BET nitrogen adsorption results. The BET surface area gives a measure of the surface area of all pores in the structure, and consequently it includes the contribution of pores that lie below the lower limit of the pore size range covered by mercury penetration experiments. Moreover, the mercury porosimetry data cannot be used for the estimation of the internal surface area of the solid unless a pattern of pore interlinking is assumed for the pore network.

The effects of calcination on the particle size were also investigated. Calcined samples prepared from 88–105 μm particles and 250–297 μm particles were resized using a Fisher electric sieve shaker. It was found that about 85% (wt. %) of the calcine retained its original size. Since some loss could be caused by abrasion during sieving, it was concluded that calcination did not influence significantly the particle size distribution.

Sulfation results

In the results presented in this section, the extent of the sulfation reaction is expressed as g SO_2 absorbed/g calcined sample

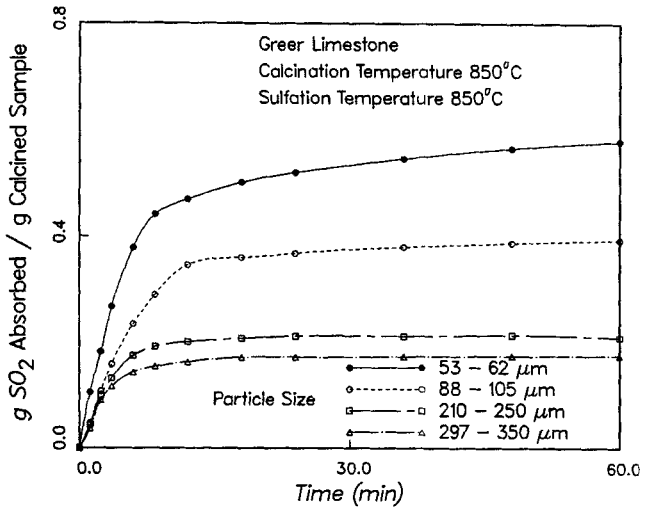

Figure 2. Dependence of conversion vs. time results on particle size.

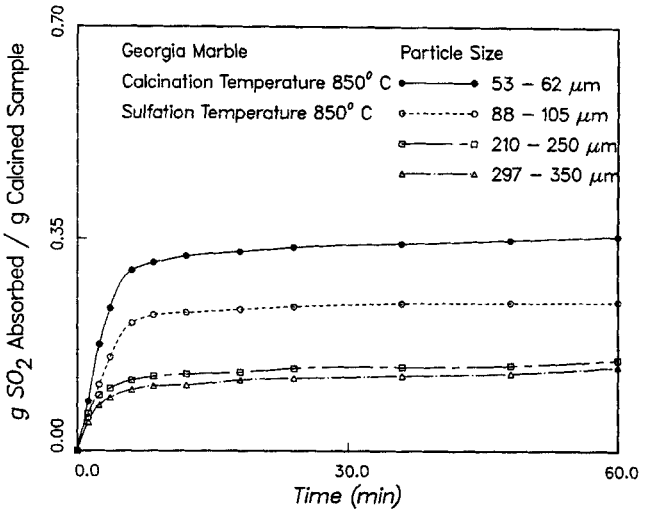

Figure 4. Dependence of conversion vs. time results on particle size.

and is computed from the obvious relationship

$$X_w = \frac{\Delta w M_{SO_2}}{w_o M_{SO_3}}$$

where Δw is the weight gain of the sample, w_o is the initial weight of the calcined sample, and M_i is the molecular weight of species i. X_w can be converted to conversion based on the calcium oxide contained in the solid through multiplication by $[M_{CaO}/(\omega_{CaO} M_{SO_2})]$, where ω_{CaO} is the weight fraction of CaO in the calcine.

The effects of particle size on the reaction trajectories (conversion vs. time curves) of particles calcined at 850°C and sulfated at 850 and 750°C are shown in Figures 2 and 3 for the Greer limestone sample and Figures 4 and 5 for the Georgia marble sample. It should be noted that since the sulfation temperatures used in all experimental results reported in Figures 2–5 were lower than the calcination temperature, it can be argued with much certainty that the initial pore structures of all calcined samples for a certain solid were the same. The results of Figures 2–5 reveal strong effects of particle size on the uptake vs. time trajectories for all pairs of sulfation and calcination temperatures studied. In general, increasing the particle size leads to lower conversion for a certain exposure time and, hence, to lower sorptive capacity and sorbent utilization. The results indicate, in view of the conclusions reached in our previous theoretical studies (Sotirchos and Yu, 1985; Yu and Sotirchos, 1987), that pore closure first takes place at the external surface of the reacting particles. This phenomenon leads to extremely high intraparticle diffusional limitations in the vicinity of the external surface of the particles, and as a result the reaction effectively ceases in the interior. Thus, notice that the conversion in the various curves of Figures 2–5 appears to reach a plateau region beyond which no noticeable change in the conversion takes place. An interesting observation that provides more support to the above conclusion is that in each figure the conversion appears to level off at about the same conversion for each curve, which is exactly what one would expect from complete pore clo-

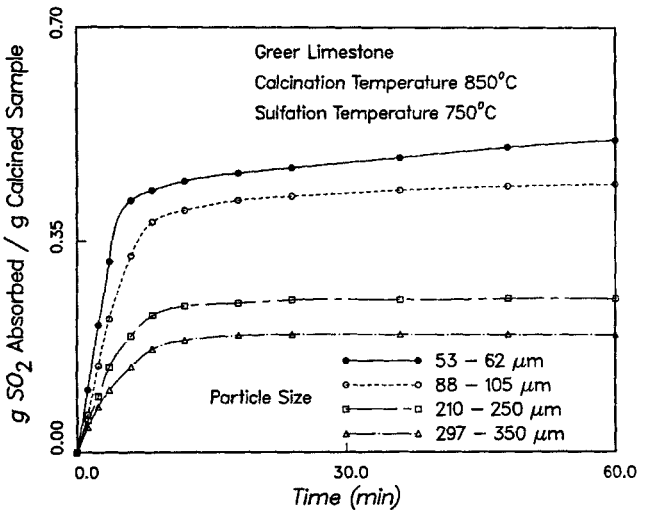

Figure 3. Dependence of conversion vs. time results on particle size.

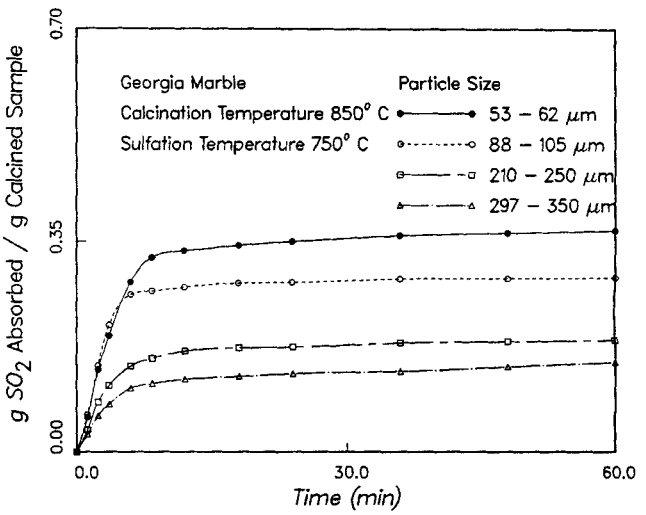

Figure 5. Dependence of conversion vs. time results on particle size.

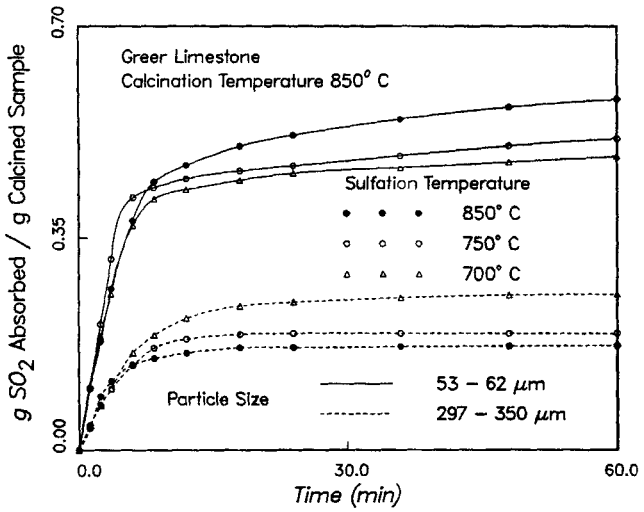

Figure 6. Dependence of conversion vs. time results on sulfation temperature and particle size.

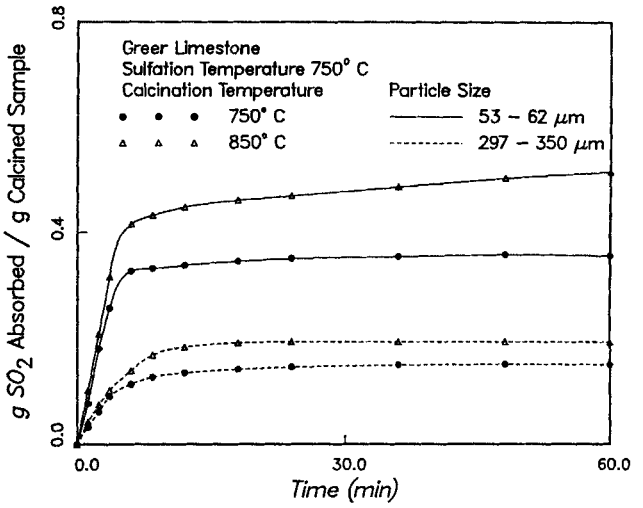

Figure 8. Dependence of conversion vs. time results on calcination temperature and particle size.

sure at the external surface of the particles provided that the external diffusional limitations are independent of particle size.

The dependence of the reaction trajectories of 53–62 and 297–350 μm particles calcined at 850°C on the sulfation temperature is shown in Figure 6 for the GL sample and in Figure 7 for the GM calcine. The results of the large particle size show diminishing conversion and sorbent utilization with increasing sulfation temperature. This result is in agreement with the pore plugging mechanism mentioned above, since an increase in the reaction (sulfation) temperature is expected to lead to higher local reaction rates in the interior of the particles through higher diffusivity in the solid product layer and higher intrinsic rate of reaction. The increased local reaction rates in turn lead to larger concentration and solid conversion gradients in the particles, and consequently to lower overall conversions when pore plugging at the external surface takes place. The maximum conversion reached by the reaction trajectories of the small marble particles, within the time interval shown in the figure, depends weakly on the sulfation temperature, indicating that these particles probably react under weak intraparticle diffusional limitations. The effects of the sulfation temperature on the reaction trajectories of the small limestone (GL sample), on the other hand, are qualitatively different. As Figure 6 shows, increasing the sulfation temperature leads to higher conversions and sorptive capacities for the 53–62 μm particles. This behavior precludes the occurrence of complete pore closure at the external surface of these particles since in such a case the opposite behavior should be observed. The higher conversions therefore must be due to the increased contribution of the large pores of the structure, Figure 1, to the total conversion after some time of reaction, because of increasing local reactivity with the sulfation temperature.

The dependence on the calcination temperature of the reaction trajectories of 53–62 and 297–350 μm particles sulfated at 750°C is shown in Figures 8 and 9 for GL and GM samples, respectively. Results for other particle sizes are given by Zarkanitis (1989). It is seen that in both cases calcination at a lower temperature leads to lower sorptive capacities. These results are not surprising since both the BET surface areas of Table 2 and

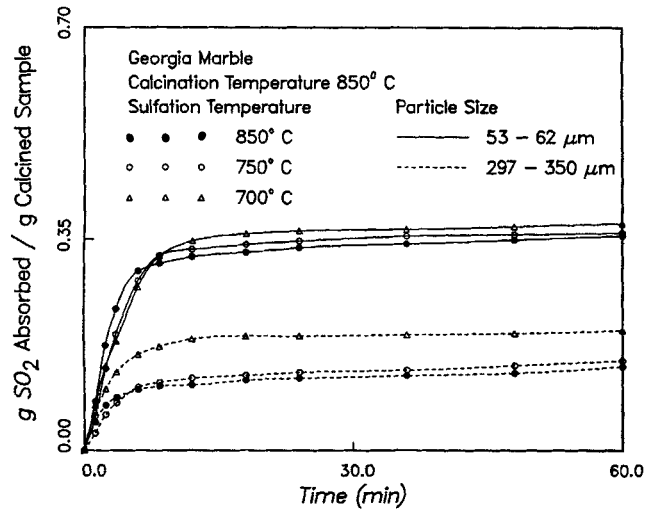

Figure 7. Dependence of conversion vs. time results on sulfation temperature and particle size.

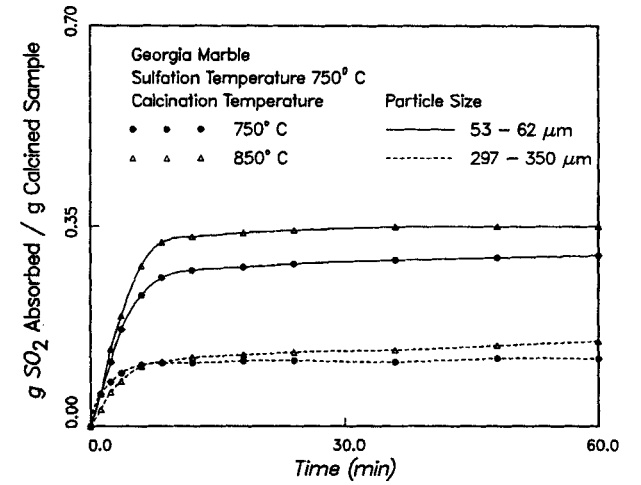

Figure 9. Dependence of conversion vs. time results on calcination temperature and particle size.

the pore size distribution of Figure 1 indicate that the pore structures of calcines produced at 750°C are characterized by larger surface areas and smaller pore sizes, and therefore by greater local reactivities and higher intraparticle diffusional limitations. The intraparticle concentration and conversion gradients are therefore greater, and when pore closure takes place at the external surface, there is more open pore space left in the interior.

It must be pointed out, however, that the results of Figures 8 and 9 should not be expected, especially for the case of the GM marble sample, if the pore size distributions of Figure 1 represent thoroughly crosslinked pore structures. The shifting of the pore size distribution toward smaller pore sizes with decreasing calcination temperature—in the case of the GM sample there is no change at all—cannot account, by itself, for the larger BET surface areas since the surface areas computed from the pore size distributions, for thoroughly crosslinked pores, are smaller than the BET values in most cases. The observed changes in internal surface area therefore must be chiefly due to pores smaller than the lower limit of the pore size range covered by mercury porosimetry. Pores of such size possess insignificant porosity and, as a result, would be plugged by solid product at very low conversion levels. Moreover, closure of these pores would have practically no effects on the intraparticle diffusion process in a thoroughly crosslinked pore structure. The interlinking characteristics of the pores of the calcines and their effects on the sulfation behavior of the solids are discussed in more detail in the following section.

Figures 10 and 11 present the variation of the 60 min sulfation capacities of the two samples used in our experiments with the particle size for all combinations of sulfation and calcination temperatures used in our experiments. The ultimate capacity for SO_2 removal predicted by the stoichiometry of the reaction for uniform plugging of the pore structure of the reacting solid with calcined product is equal to 0.60 and 0.57 g SO_2/g calcined sorbent for the GL and GM samples, respectively. In accordance with the results presented and discussed thus far, the 60 min capacity of the stones appears in general to decrease with increasing sulfation temperature and particle size and decreasing calcination temperature. Notice that the 60 min capacities

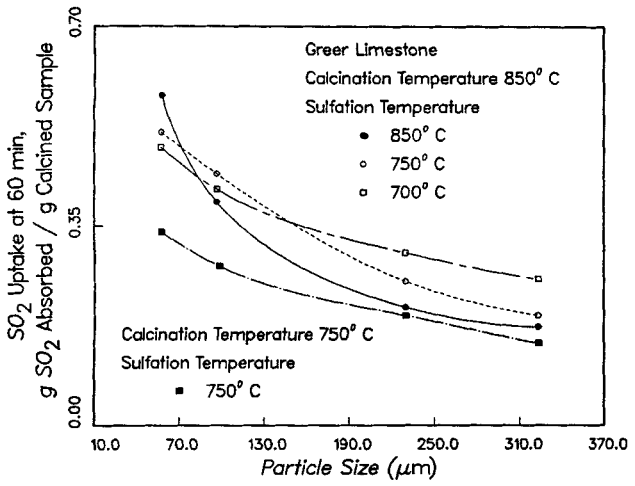

Figure 10. Variation of 60 min sulfation capacity with particle size, sulfation temperature, and calcination temperature.

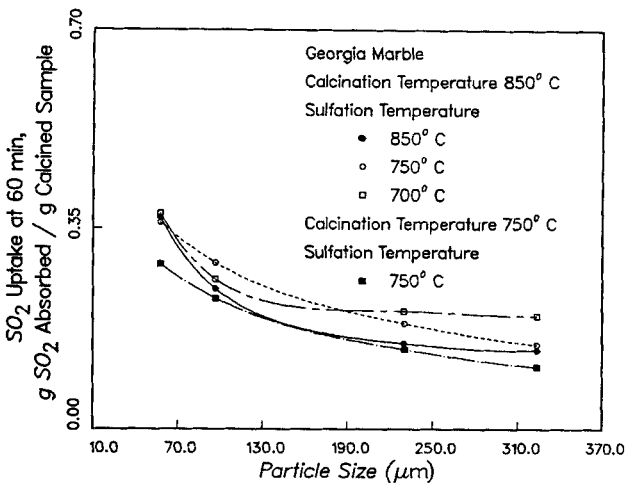

Figure 11. Variation of 60 min sulfation capacity with particle size, sulfation temperature, and calcination temperature.

of Figures 10 and 11 are in general well below the maximum stoichiometrically allowable conversions mentioned above. For the GM sample this is true even for the 53–62 μm particles calcined at 850°C.

An interesting observation is that the sulfation capacities of the Georgia marble particles are always much lower than those of their Greer limestone counterparts although the initial reactivities of the two solids do not appear to be much different (compare the initial slopes of the various conversion vs. time curves) and their pore size distributions are qualitatively similar. One could argue that these differences are due to the smaller pore sizes of the GM samples (compare curves *A* and *B* in Figure 1), which cause higher resistance for intraparticle mass transport and lead to plugging of the external surface of the particles by solid product at lower average conversions. Such an argument, however, does not provide an explanation as to why the conversions reached by the 53–62 μm marble particles for large reaction times are insignificantly influenced by the sulfation temperature, a behavior characteristic of reaction under kinetically controlled conditions. An increase in the sulfation temperature generally leads to higher local reactivity (because of increasing intrinsic reactivity and product layer diffusivity), and under conditions of significant intraparticle diffusional limitations it should cause steeper conversion profiles and hence plugging of the external surface at lower average conversions.

The initial value of the observable modulus $R_{obs}a^2/(c_bD^e)$ that is computed from the experimental data is about 0.25 for the small GM particles (53–62 μm), further indicating that the process starts in the kinetically controlled regime (Hudgins, 1968). (R_{obs} is the observed reaction rate, a is the particle radius, c_b is the bulk concentration of SO_2, and D^e is the intraparticle diffusion coefficient computed for a thoroughly interconnected pore structure using the Feng and Stewart [1973] flux model.) However, noncatalytic gas-solid reactions with solid product can exhibit ultimate conversions that are lower than the stoichiometrically allowable, even in the absence of intraparticle diffusional limitations. This situation results when the feeder pores of a cavity or of a cluster of large pores in an aperture-cavity pore structure are filled with solid product, causing the formation of inaccessible pore space. The occurrence of this phenomenon was

amply demonstrated by the simulation results of Yu and Sotirchos (1987), who used a population of randomly inteconnected short pores to represent the structure of the porous solid. The structural model developed by these investigators will be used, along with a model for diffusion and reaction in the intraparticle pore space, to analyze some of the sulfation results obtained for the Georgia marble sample in this study.

Comparison with predictions of a distributed pore model for gas-solid reactions

The generalized pore model of Yu and Sotirchos (1987) considers a pore network structure built around a three-dimensional lattice with the bonds of the lattice functioning as axes of the pore segments in the network. The pore network is described by the pore size distribution of the pore segments and the coordination number of the lattice, z, the latter being defined as the average number of pores emanating from a site. The length of the pore segments is assumed to be distributed independently of the pore size. For a given lattice structure, the coordination number determines the accessibility of the network, that is, the functional relationship between the number fraction of open pores and the number fraction of open pores that belong to inaccessible clusters of pores. There is a minimum number fraction of open pores, referred to as the percolation threshold of the structure, below which all open pores belong to inaccessible clusters, and consequently diffusion and reaction cannot take place in the pore structure. For infinitely large coordination number, a thoroughly inteconnected pore structure is obtained, and the equations of the generalized pore model reduce to those describing evolution in a pore structure consisting of randomly overlapping, infinitely long cylindrical capillaries (Sotirchos and Yu, 1985). Readers interested in the details of the generalized random pore model are advised to consult the paper by Yu and Sotirchos (1987).

The predictions of the generalized pore model are shown in Figure 12 for Georgia marble particles calcined and sulfated at 850°C. A Bethe tree (Fisher and Essam, 1961) was used to obtain the accessibility function of the pore network, and two values of the coordinate number were employed, $z = 6$ (dashed curves) and $z = \infty$ (solid curves). The use of a Bethe tree structure does not limit the applicability of the results presented here since most two- and three-dimensional lattices have accessibility functions of similar shape. In other words, for a different lattice structure one can find a coordination number that will produce an accessibility function similar, qualitatively and quantitatively, to that of Bethe trees for $z = 6$. No other adjustable parameters were employed in producing the results shown in the figure. On the basis of values reported in previous experimental and theoretical studies, the solid product layer diffusivity in the product layer was taken equal to 2×10^{-12} m^2/s. The intraparticle diffusivity was computed using the flux model of Burganos and Sotirchos (1987) and the pore size distribution data of Figure 1. This flux model is compatible with the network structure of the generalized pore model, and for infinitely large coordination number, it reduces, as expected, to the flux model of Feng and Stewart (1973). The intraparticle effective diffusivities computed were 5.23×10^{-7} and 2.32×10^{-6} m^2/s for $z = 6$ and $z = \infty$, respectively. A first-order reaction was assumed, and the reaction rate constant was computed through nonlinear regression using the analytical expression for the initial rate of reaction under pseudosteady-state conditions and the measured initial rates of reaction for the four particle sizes. The reaction rate constants obtained through this procedure were 1.651×10^{-5} and 1.344×10^{-5} m/s for $z = 6$ and $z = \infty$, respectively. Details on the estimation of the various parameters and the procedures used are given by Zarkanitis (1989).

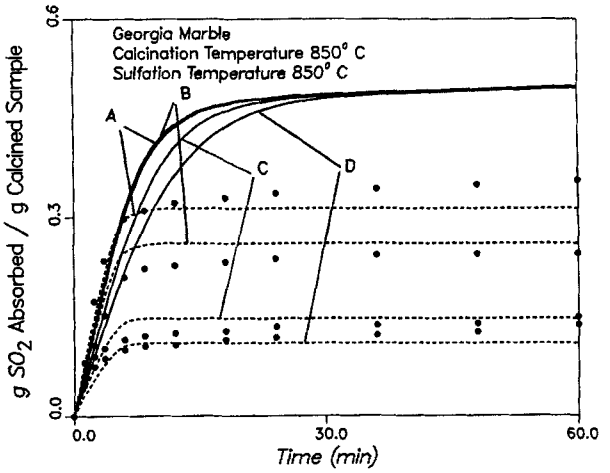

Figure 12. Comparison of experimental results of Figure 4 with predictions of the random pore model of Yu and Sotirchos (1987).

— $z = \infty$; --- $z = 6$
A 53–62 μm; *B* 88–105 μm; *C* 210–250 μm; *D* 297–350 μm

The reaction trajectories predicted by the generalized random pore model for $z = 6$ (dashed curves in Figure 12) provide a good approximation to the experimental data (solid circles). The ultimate conversion reached by the smallest particle is lower than that predicted by the stoichiometry of the reaction for complete pore plugging mainly because of the formation of inaccessible pore space. For the other particle sizes, the ultimate conversion is also limited by pore closure at the external surface while open, accessible pore space is left in the interior. Complete pore closure takes place at the external surface of the particles because the intraparticle diffusional limitations for $z = 6$ are stronger. Not only is the intraparticle diffusion coefficient initially about four times smaller than that for thoroughly crosslinked pores, but its value decreases rapidly as closure of the small pores and formation of inaccessible pore space starts to take place. The results for $z = \infty$ (solid curves in Figure 12) clearly demonstrate that if a thoroughly inteconnected pore network is assumed, the distributed pore model is incapable of reproducing the experimental data. Because of the presence of the large pores, Figure 1, the intraparticle diffusion coefficient decreases more slowly with the conversion than the reactivity of the solid. The reaction eventually moves into the kinetically controlled regime, and the conversion vs. time curves for all particles approach each other. The two smaller particles start reacting under weak intraparticle diffusional limitations—the observable modulus for the smallest particle is initially equal to about 0.25—and as a result their conversion histories are practically indistinguishable.

If formation of inaccessible pore space is not considered, the predictions of the random pore model can be made to agree with the experimental data only by using artificially low values of effective diffusivity that are inconsistent with the pore structure assumed in the construction of the structural model. This is essentially what is usually done in the literature when simplified

pore or grain models are successfully used to reproduce experimental data for noncatalytic reactions with solid product. The generalized random pore model performed similarly for the GL samples, but for higher values of coordination number—indicating that that the capacity of limestones for SO_2 removal is influenced not only by the qualitative and quantitative features of their pore size distributions but also by the connectedness of their pore space. Considering the different petrographic texture of the parent rocks of the two calcines, the observed differences in their pore size distribution and the connectedness of their pore space are not surprising.

It should be pointed out that a rigorous application of the generalized pore model requires correction of the pore size distribution that is calculated from mercury porosimetry data for a thoroughly interconnected pore network or, equivalently, for a structure of infinitely long pores. This correction is needed because in a network of finite pore segments, a large pore is filled by mercury at a capillary pressure determined not by its own radius but by the radius of the feeder pore through which it is invaded by mercury. The correction of the pore size distribution requires, among other things, the distribution of the length of the pores and the particle size of the sample used to obtain the mercury intrusion results, or the use of an unknown parameter (Mishra and Sharma, 1988) that accounts for their effects on the mercury intrusion curve. Since we did not want to employ an additional parameter, the uncorrected pore size distribution of Figure 1 (solid *B* curve) was used to obtain the results of Figure 12. This, however, does not in any way affect the validity of the conclusions reached in our study from the comparison of simulation results and experimental data. The main difference between the uncorrected and corrected pore size distributions (Mishra and Sharma, 1988) is that in the latter, part of the pore volume from the intermediate pore size range is shifted to larger pore sizes. As a result, slightly different coordination numbers have to be used in order to obtain reaction trajectories similar to those computed using the uncorrected pore size distribution (Zarkanitis, 1989).

Conclusions

Calcination and sulfation experiments were carried out using two stones of very high calcium carbonate content, a limestone and a calcitic marble. The experimental results showed little dependence of the total porosity of the calcined product on the calcination temperature in the range 750–850°C, but the BET surface area of both calcines decreased with increasing calcination temperature. The pore size distribution of the calcined limestone, measured by mercury porosimetry, shifted toward larger pore sizes with increasing calcination temperature, while that of the calcined marble remained practically unchanged. The sulfation experiments showed strong dependence of the conversion vs. time results on the particle size, calcination temperature, sulfation temperature, and limestone type. Specifically, the conversion attained after some reaction time decreased with increasing particle size, decreasing calcination temperature, and increasing sulfation temperature. It is believed that this behavior is the result of increasing diffusional limitations in the intraparticle region, which lead to lower average conversions when plugging of the pores takes place at the external surface of the particles.

One of the most important findings of our study was that the ultimate capacity of the marble sample for SO_2 removal was considerably lower than that of the limestone although the initial reactivities of their calcined products appeared to be similar, they had approximately the same CaO content and porosity, and their initial internal surface areas were similar. An explanation for these differences could be found in the smaller pore sizes (obtained by mercury porosimetry) of the marble samples, but the above observation was true even for the smallest marble particles used in our experiments (53–62 μm), whose reaction trajectories appear to depend rather weakly on the sulfation temperature, thus indicating absence of strong intraparticle diffusional limitations. We thus believe that the above behavior must be due to the aperture-cavity structure of the pore space of the calcines, which may lead to formation of inaccessible pore space when closure of the small pores of the structure takes place. The formation of inaccessible pore space may be experimentally investigated by measuring apparent densities and pore size distributions of partially reacted samples (by mercury porosimetry or gas adsorption). However, much larger samples than those used in TGA experiments are needed for an accurate measurement of these quantities.

Acknowledgment

This work was supported by a grant from the U. S. Department of Energy.

Literature Cited

Borgwardt, R. H., "Kinetics of the Reaction of SO_2 with Calcined Limestone," *Environ. Sci. Technol.*, **4**, 59 (1970).

Borgwardt, R. H., and R. D. Harvey, "Properties of Carbonate Rocks Related to SO_2 Reactivity," *Environ. Sci. Technol.*, **6**, 350 (1972).

Borgwardt, R. H., W. F. Roache, and K. R. Bruce, "Method for Variation of Grain Size in Studies of Gas-Solid Reactions," *Ind. Eng. Chem. Fund.*, **25**, 165 (1986).

Burganos, V. N., and S. V. Sotirchos, "Diffusion in Pore Networks: Effective-Medium Theory and Smooth Field Approximation," *AIChE J.*, **33**, 1678 (1987).

Chan, R. K., K. S. Murthi, and D. Harrison, "Thermogravimetric Analysis of Ontario Limestones and Dolomites. II: Reactivity of Sulfur Dioxide with Calcined Samples," *Can. J. Chem.*, **48**, 2979 (1970).

Christman, P. G., and T. F. Edgar, "Distributed Pore Size Model for Sulfation of Limestone," *AIChE J.*, **29**, 388 (1983).

Crowley, J. A., "A Reaction/Adsorption System for Gas-Solid Reaction Studies," M.S. Thesis, Univ. Rochester (1985).

Dogu, T., "The Importance of Pore Structure and Diffusion in the Kinetics of Gas-Solid Noncatalytic Reactions: Reaction of Calcined Limestone with SO_2," *Chem. Eng. J.*, **21**, 213 (1981).

Feng, C., and W. E. Stewart, "Practical Models for Isothermal Diffusion and Flow in Porous Solids," *AIChE J.*, **12**, 143 (1973).

Fisher, M. E., and J. W. Essam, "Some Cluster Size and Percolation Problems," *J. Math. Phys.*, **2**, 609 (1961).

Gregg, S. J., and K. S. W. Sing, *Adsorption, Surface Area, and Porosity*, Academic Press, New York (1982).

Hartman, M., and R. W. Coughlin, "Reaction of Sulfur Dioxide with Limestone and the Influence of Pore Structure," *Ind. Eng. Chem. Process Des. Dev.*, **13**, 248 (1974).

———, "Reaction of Sulfur Dioxide with Limestone and the Grain Model, *AIChE J.*, **22**, 490 (1976).

Harrington, R. E., R. H. Borgwardt, and A. E. Potter, "Reactivity of Selected Limestones and Dolomites with Sulfur Dioxide," *Amer. Ind. Hyg. Assoc. J.*, **29**, 152 (1968).

Hartman, M., J. Pata, and R. W. Coughlin, "Influence of Porosity of Calcium Carbonates on Their Reactivity with Sulfur Dioxide," *Ind. Eng. Chem. Process Des. Dev.*, **17**, 411 (1978).

Hasler, J. R., et al., "Testing of Limestone Samples from the TVA Region as Sulfur Dioxide Sorbents in Atmospheric Fluidized-Bed Combustors (Technical Report)," Inst. Mining Mineral Res., Univ. Kentucky (1984).

Hudgins, R. R., "A General Criterion for Absence of Diffusion Control in an Isothermal Catalyst Pellet," *Chem. Eng. Sci.*, **23**, 23 (1968).

Marsh, D. W., and D. L. Ulrichson, "Rate and Diffusional Study of the Reaction of Calcium Oxide with Sulfur Dioxide," *Chem. Eng. Sci.*, **40,** 423 (1985).
Mishra, B. K., and M. M. Sharma, "Measurement of Pore Size Distributions from Capillary Pressure Curves," *AIChE J.*, **34,** 684 (1988).
Nelsen, F. M., and F. T. Eggertsen, "Determination of Surface Area and Adsorption Measurements by a Continuous Flow Method," *Anal. Chem.*, **30,** 1387 (1958).
Sotirchos, S. V., and H. C. Yu, "Mathematical Modeling of Gas-Solid Reactions with Solid Product," *Chem. Eng. Sci.*, **40,** 2039 (1985).
Sotirchos, S. V., J. A. Crowley, and H. C. Yu, "A Reaction/Adsorption Device for Gas-Solid Reaction Studies," *Chem. Eng. Commun.*, **71,** 88 (1988).
Vogel, G. J., et al., Quarterly Rept. (Jan.–Mar. 1977), prepared for DOE, Argonne Nat. Lab. (1977).
Yu, H. C., and S. V. Sotirchos, "A Generalized Pore Model for Gas-Solid Reactions with Pore Closure Behavior," *AIChE J.*, **33,** 382 (1987).
Zarkanitis , S., "Pore Structure and Reactivity Evolution during Limestone Sulfation," Ph.D. Thesis, Univ. Rochester (1989).

Manuscript received Apr. 12, 1988, and revision received Jan. 10, 1989.